The Astrophysical Journal Letters, 973:L48 (9pp), 2024 October 1 https://doi.org/10.3847/2041-8213/ad5a8c


# Metis Observation of the Onset of Fully Developed Turbulence in the Solar Corona

Daniele Telloni[1,41], Luca Sorriso-Valvo[2,3,4,41], Gary P. Zank[5,6], Marco Velli[7], Vincenzo Andretta[8], Denise Perrone[9], Raffaele Marino[10], Francesco Carbone[11], Antonio Vecchio[12,13], Laxman Adhikari[5], Lingling Zhao[5], Sabrina Guastavino[14], Fabiana Camattari[1,14], Chen Shi[7], Nikos Sioulas[7], Zesen Huang[7], Marco Romoli[15], Ester Antonucci[1], Vania Da Deppo[16], Silvano Fineschi[1], Catia Grimani[17,18], Petr Heinzel[19,20], John D. Moses[21], Giampiero Naletto[22], Gianalfredo Nicolini[1], Daniele Spadaro[23], Marco Stangalini[9], Luca Teriaca[24], Michela Uslenghi[25], Lucia Abbo[1], Frédéric Auchère[26], Regina Aznar Cuadrado[24], Arkadiusz Berlicki[20,27], Roberto Bruno[28], Aleksandr Burtovoi[29], Gerardo Capobianco[1], Chiara Casini[1,16,30], Marta Casti[31], Paolo Chioetto[16,29], Alain J. Corso[16], Raffaella D'Amicis[28], Yara De Leo[24,32], Michele Fabi[17,18], Federica Frassati[1], Fabio Frassetto[16], Silvio Giordano[1], Salvo L. Guglielmino[23], Giovanna Jerse[33], Federico Landini[1], Alessandro Liberatore[34], Enrico Magli[35], Giuseppe Massone[1], Giuseppe Nisticò[36], Maurizio Pancrazzi[1], Maria G. Pelizzo[37], Hardi Peter[24], Christina Plainaki[9], Luca Poletto[16], Fabio Reale[38,39], Paolo Romano[23], Giuliana Russano[8], Clementina Sasso[8], Udo Schühle[24], Sami K. Solanki[24], Leonard Strachan[40], Thomas Straus[8], Roberto Susino[1], Rita Ventura[23], Cosimo A. Volpicelli[1], Joachim Woch[24], Luca Zangrilli[1], Gaetano Zimbardo[36], and Paola Zuppella[16]

[1] National Institute for Astrophysics, Astrophysical Observatory of Torino, Via Osservatorio 20, I-10025 Pino Torinese, Italy; daniele.telloni@inaf.it
[2] National Research Council, Institute for the Science and Technology of Plasmas, Via Amendola 122/D, I-70126 Bari, Italy
[3] Space and Plasma Physics, School of Electrical Engineering and Computer Science, KTH Royal Institute of Technology, Teknikringen 31, SE-114 28 Stockholm, Sweden
[4] Swedish Institute of Space Physics, Ångström Laboratory, Lägerhyddsvägen 1, SE-751 21 Uppsala, Sweden
[5] Center for Space Plasma and Aeronomic Research, University of Alabama in Huntsville, Huntsville, AL 35805, USA
[6] Department of Space Science, University of Alabama in Huntsville, Huntsville, AL 35805, USA
[7] Earth, Planetary, and Space Sciences, University of California, Los Angeles, CA 90095, USA
[8] National Institute for Astrophysics, Astronomical Observatory of Capodimonte, Salita Moiariello 16, I-80131 Napoli, Italy
[9] Italian Space Agency, Via del Politecnico snc, I-00133 Roma, Italy
[10] Laboratoire de Mécanique des Fluides et d'Acoustique, Centre National de la Recherche Scientifique, École Centrale de Lyon, Université Claude Bernard Lyon 1, INSA de Lyon, F-69134 Écully, France
[11] National Research Council, Institute of Atmospheric Pollution Research, c/o University of Calabria, I-87036 Rende, Italy
[12] Radboud Radio Lab, Department of Astrophysics, Radboud University, NL-6500 Nijmegen, The Netherlands
[13] Laboratoire d'Etudes Spatiales et d'Instrumentation en Astrophysique, Observatoire de Paris, Université Paris Sciences et Lettres, Centre National de la Recherche Scientifique, Sorbonne Université, Université Paris Diderot, Sorbonne Paris Cité, 5 Place Jules Janssen, F-92195 Meudon, France
[14] University of Genoa, Department of Mathematics, Via Dodecaneso 35, I-16146 Genoa, Italy
[15] University of Florence, Department of Physics and Astronomy, Via Giovanni Sansone 1, I-50019 Sesto Fiorentino, Italy
[16] National Research Council, Institute for Photonics and Nanotechnologies, Via Trasea 7, I-35131 Padova, Italy
[17] University of Urbino Carlo Bo, Department of Pure and Applied Sciences, Via Santa Chiara 27, I-61029 Urbino, Italy
[18] National Institute for Nuclear Physics, Section in Florence, Via Bruno Rossi 1, I-50019 Sesto Fiorentino, Italy
[19] Czech Academy of Sciences, Astronomical Institute, Fričova 298, CZ-25165 Ondřejov, Czechia
[20] University of Wrocław, Centre of Scientific Excellence—Solar and Stellar Activity, ul. Kopernika 11, PL-51-622 Wrocław, Poland
[21] National Aeronautics and Space Administration, Headquarters, Washington, DC 20546, USA
[22] University of Padua, Department of Physics and Astronomy, Via Francesco Marzolo 8, I-35131 Padova, Italy
[23] National Institute for Astrophysics, Astrophysical Observatory of Catania, Via Santa Sofia 78, I-95123 Catania, Italy
[24] Max Planck Institute for Solar System Research, Justus-von-Liebig-Weg 3, D-37077 Göttingen, Germany
[25] National Institute for Astrophysics, Institute of Space Astrophysics and Cosmic Physics of Milan, Via Alfonso Corti 12, I-20133 Milano, Italy
[26] Université Paris-Saclay, Centre National de la Recherche Scientifique, Institut d'Astrophysique Spatiale, Rue Jean-Dominique Cassini, F-91440 Bures-sur-Yvette, France
[27] University of Wrocław, Astronomical Institute, Kopernika 11, PL-51622 Wrocław, Poland
[28] National Institute for Astrophysics, Institute for Space Astrophysics and Planetology, Via del Fosso del Cavaliere 100, I-00133 Roma, Italy
[29] National Institute for Astrophysics, Astrophysical Observatory of Arcetri, Largo Enrico Fermi 5, I-50125 Firenze, Italy
[30] Centre of Studies and Activities for Space "Giuseppe Colombo," Via Venezia 15, I-35131 Padova, Italy
[31] The Catholic University of America at the National Aeronautics and Space Administration, Goddard Space Flight Center, Greenbelt, MD 20771, USA
[32] University of Catania, Department of Physics and Astronomy, Via Santa Sofia 64, I-95123 Catania, Italy
[33] National Institute for Astrophysics, Astronomical Observatory of Trieste, Località Basovizza 302, I-34149 Trieste, Italy
[34] Jet Propulsion Laboratory, California Institute of Technology, Pasadena, CA 91109, USA
[35] Politecnico of Turin, Department of Electronics and Telecommunications, Corso Duca degli Abruzzi 24, I-10129 Torino, Italy
[36] University of Calabria, Department of Physics, Ponte Pietro Bucci Cubo 31C, I-87036 Rende, Italy
[37] University of Padua, Department of Information Engineering, Via Giovanni Gradenigo 6, I-35131 Padova, Italy
[38] University of Palermo, Department of Physics and Chemistry—Emilio Segrè, Piazza del Parlamento 1, I-90134 Palermo, Italy
[39] National Institute for Astrophysics, Astronomical Observatory of Palermo, Piazza del Parlamento 1, I-90134 Palermo, Italy
[40] Naval Research Laboratory, Space Science Division, Washington, DC 20375, USA

*Received 2023 November 1; revised 2024 May 6; accepted 2024 May 31; published 2024 September 26*



[41] These authors contributed equally to this work.

**Abstract**

This Letter reports the first observation of the onset of fully developed turbulence in the solar corona. Long time series of white-light coronal images, acquired by Metis aboard Solar Orbiter at 2 minutes cadence and spanning about 10 hr, were studied to gain insight into the statistical properties of fluctuations in the density of the coronal plasma in the time domain. From pixel-by-pixel spectral frequency analysis in the whole Metis field of view, the scaling exponents of plasma fluctuations were derived. The results show that, over timescales ranging from 1 to 10 hr and corresponding to the photospheric mesogranulation-driven dynamics, the density spectra become shallower moving away from the Sun, resembling a Kolmogorov-like spectrum at 3 $R_\odot$. According to the latest observation and interpretive work, the observed $5/3$ scaling law for density fluctuations is indicative of the onset of fully developed turbulence in the corona. Metis observation-based evidence for a Kolmogorov turbulent form of the fluctuating density spectrum casts light on the evolution of 2D turbulence in the early stages of its upward transport from the low corona.

*Unified Astronomy Thesaurus concepts:* Magnetohydrodynamics (1964); Interplanetary turbulence (830); Space plasmas (1544); Solar corona (1483); Solar wind (1534)

## 1. Introduction

Turbulence, or the complex and apparently disordered motion of natural fluids, is a physical phenomenon that pervades the Universe, developing in terrestrial and space environments over a wide range of scales, from oceanic (e.g., Carbone et al. 2016; Huang & Wang 2019) and atmospheric (e.g., Marino et al. 2022; Carbone et al. 2022a) flows, to the dynamics of gas forming interstellar nebulae (e.g., Kritsuk et al. 2011; Federrath & Klessen 2012) and the intracluster medium (e.g., Schekochihin & Cowley 2006). Despite its ubiquity and progress in the field, as Nobel Laureate in physics Richard Feynman remarked, turbulence remains "the most important unsolved problem of classical physics" (Feynman et al. 1963). Indeed, being a nonlinear phenomenon, it implies that different modes do mutually exchange energy across different length scales, making its analytical description challenging. In addition, turbulence is a nonequilibrium process (both dynamically and energetically), and therefore its study in statistical/thermodynamic terms is very complex and still under exploration (e.g., Gallavotti & Cohen 1995), as recently shown for the solar photosphere (e.g., Viavattene et al. 2020, 2021). Finally, although it can be characterized, in a statistical sense, by particularly ordered structures, turbulence is highly chaotic with many degrees of freedom (Bohr et al. 1998), limiting the applicability of standard chaos theories, known to work satisfactorily only for systems with a few degrees of freedom (e.g., Carbone et al. 2021, 2022b).

According to the phenomenology à la Richardson, turbulence is initiated at large scales by the injection of energy into the flow system by external forcing, such as large-scale shears or instabilities. At intermediate scales, energy is transferred conservatively through a hierarchy of eddies along the turbulent cascade, down to smaller structures. Finally, when the energy reaches the sub-ion scales, it gets dissipated into heat by viscous stresses. Three different ranges of scales can therefore be identified, corresponding to the injection, inertial (or fluid) and dissipative (or kinetic) regimes. These are characterized by different scalings of the power spectral density of the fluctuations, and separated by spectral breaks. Specifically, according to the Kolmogorov theory of turbulence (Kolmogorov 1941), the inertial-range energy spectrum of a turbulent fluid scales with the wavenumber $k$ as $k^{-5/3}$, a feature regarded as distinctive of fully developed turbulence. The so-called Kolmogorov's $-5/3$ scaling law can be easily retrieved under the hypothesis of a constant energy transfer rate $\epsilon$ in the inertial range. Since the turnover time $\tau$ for an eddy of size $\ell$can be dimensionally obtained as $\tau \sim \ell/v \sim 1/kv$ (with $v$ being the rms velocity fluctuation), while its energy density is $\sim v^2$, the rate of energy flux $\epsilon \sim v^2/\tau$ is therefore $\sim v^3 k$. It follows that the energy spectral density $E \sim v^2/k$ scales as $E \sim \epsilon^{2/3} k^{-5/3}$. The reader is referred to Frisch (1995) for a complete and exhaustive description of hydrodynamic turbulence and its properties, and to the recent review by Marino & Sorriso-Valvo (2023) on the scaling laws for energy transfer in space plasma turbulence.

Among the many natural frameworks in which the Kolmogorov energy spectrum has been observed, the solar wind holds a prominent place. The continuous stream of magnetized particles emitted by the Sun (Hundhausen 1972) is indeed known to be in a fully developed turbulent state since the seminal work by Coleman (1968) and is rightfully considered the largest turbulence laboratory (Bruno & Carbone 2013). Indeed, since the beginning of the space era, the solar wind has been probed by a flotilla of robotic spacecraft that have measured its properties over a wide range of spatial scales (Verscharen et al. 2019), advancing the understanding of this fundamental physical process (see, e.g., the review by Tu & Marsch 1995, and references therein). Last to be launched in 2018 and 2020, respectively, were Parker Solar Probe (Fox et al. 2016) and Solar Orbiter (Müller et al. 2020). Central to these space missions, which will get closer than ever before to the Sun, carrying a full set of remote-sensing and in situ instruments, is unveiling the origin of turbulence in the solar wind and assessing whether and to what extent it contributes to plasma heating (Telloni et al. 2023a).

Thanks to measurements by Parker Solar Probe, which repeatedly flies inside the solar corona, it is now established that solar wind turbulence originates in the outermost layers of the Sun's atmosphere (Zank et al. 2022; Zhao et al. 2022), and it evolves during the expansion in the heliosphere toward a fully developed state (Telloni et al. 2021). In particular, radio scintillation observations (Lotova et al. 1985) supported by magnetohydrodynamic (MHD) simulations (Chhiber et al. 2019), indicate enhanced turbulence at about 10–20 $R_\odot$ ($1\ R_\odot = 6.96 \times 10^5$ km) around the Alfvén surface (i.e., where solar wind and Alfvén speeds are equal), which ideally marks the transition from the magnetically dominated corona to the dynamically dominated solar wind region (see also Réville & Brun 2017). The turbulence enhancement at the Alfvén point is, on the other hand, also predicted by simple considerations by starting from the equation for Alfvén wave propagation and

solving it in the Wentzel–Kramers–Brillouin limit to get an analytical expression for the conservation of wave action flux (Velli 1993; Telloni et al. 2023a). However, models for the mechanisms underlying the onset of turbulence in the corona are still a matter of strong debate. They basically come in two different paradigms. In one possible scenario, originally introduced by Matthaeus et al. (1999), quasi-2D incompressible turbulence is produced by the nonlinear interactions between Alfvén wave fluxes, emanating from the photosphere by convection-related jostling of open magnetic flux tubes, and counterpropagating modes, reflected back toward the Sun by coronal stratification (see also Verdini et al. 2009). As an alternative turbulence model, in the nearly incompressible (NI) MHD theory (Zank et al. 2017, 2018, 2020), quasi-2D turbulent fluctuations are generated through reconnection processes in the constantly emerging magnetic carpet (Title & Schrijver 1998) and advected upward by the coronal flow. A discussion of the two turbulence models along with the related distinguishing features can be found in Zank et al. (2021).

With the exception of occasional local measurements by Parker Solar Probe during its brief incursions into the corona (Kasper et al. 2021), the Sun's atmosphere in the region of the nascent solar wind can only be probed remotely with spectroscopic or imaging instruments, such as coronagraphs. Space-borne imaging instruments provide primarily density-related observations. However, within the NI MHD turbulence theory, the density fluctuations can be considered as entropic modes (i.e., structures passively transported by quasi-2D incompressible turbulence), and thus be a proxy for the turbulence associated with velocity field fluctuations. A trivial demonstration that, under the assumption that density is a passive scalar, its fluctuations can give rise to a Kolmogorov-like turbulent spectrum stems from the Yaglom's law (Frisch 1995), which can be written as $\langle \Delta u \Delta \rho^2 \rangle = -4/3\epsilon\ell$, where $\Delta u$ and $\Delta \rho$ denote velocity and density fluctuations, respectively. If the velocity fluctuations are assumed to follow the Kolmogorov phenomenology, namely $\Delta u \sim \ell^{1/3}$, the Yaglom's law predicts that $\Delta \rho \sim \ell^{1/3}$ as well, which corresponds to the Kolmogorov scaling law. Zank et al. (2023) developed a novel method for distinguishing between wave and advected modes and found that entropic density fluctuations are typically dominant in the solar wind plasma. More importantly, Zank et al. (2022) provided evidence that the density fluctuations sampled by Parker Solar Probe during its first passage inside the solar corona are not due to magnetosonic modes, but most likely are entropic fluctuations, and thus indicative of turbulence.

Most earlier studies of coronal density fluctuations have focused on the detection of periodic or quasiperiodic wavelike phenomena (e.g., Ofman et al. 2000; Morgan et al. 2004; Telloni et al. 2013, 2014) or recurrent density transients (Ventura et al. 2023) superimposed on the spectrum of background fluctuations. Much less attention, however, has been devoted to the latter. A few attempts have been made in Telloni et al. (2009a, 2009b) exploiting data gathered with the UltraViolet Coronagraph Spectrometer (Kohl et al. 1995) aboard the Solar and Heliospheric Observatory (Domingo et al. 1995), but the results were affected by significant background noise at timescales of less than 3 hr (which suggested only large-scale scaling laws probably associated with nonpropagating tangential discontinuities observed during solar rotation) and restricted by the limited field of view of the instrument. The high spatial and temporal resolution measurements of coronal white-light emission by the Metis coronagraph (Fineschi et al. 2020; Antonucci et al. 2020b) aboard Solar Orbiter, combined with its unprecedentedly high signal-to-noise ratio, provide the opportunity to explore the properties of density spectra in the whole solar corona. This Letter reports the output of a statistical analysis of such measurements to address temporal fluctuations only and to ascertain for the first time the presence of fully developed turbulence in coronal flows. The analysis and results are presented in Section 2, while final remarks on how the present findings can be regarded as a critical discriminant in the two competing turbulence models for solar coronal heating are outlined in Section 3.

## 2. Analysis and Results

On 2022 October 12, Solar Orbiter was at its fifth perihelion, orbiting at only 0.29 au from the Sun. From 10:15 to 20:16 UT, Metis observed continuously the solar corona in visible light (VL) between 580 and 640 nm. This resulted in a 10 hr database of 298 coronal brightness (B) images at 2 minute cadence. During these observations, the instrument field of view (FOV) ranged from 1.75 to 3.15 $R_\odot$. The average of the images collected by Metis, cleared of corrupted ones (4% in total, which were removed from the time series, then interpolated) and calibrated in units of mean solar disk brightness $B_\odot$ according to Liberatore et al. (2023) and De Leo et al. (2023), is illustrated in Figure 1(a). Note that Metis images are oriented in such a way as to have the rotation axis aligned with the vertical. Just for visualization purposes, in order to sharpen the boundaries separating different large-scale magnetic structures, the difference of Gaussians (DoG) filter, a commonly used algorithm for edge enhancement (see, e.g., Morgan & Druckmüller 2014), is applied to Figure 1(a). The result is shown in Figure 1(b). The spectral analysis is performed on original unfiltered data, i.e., on total brightness measurements from Metis not previously reprocessed by means of the DoG filter so as not to remove coronal background that may contain important signal information.

Before dwelling into the analysis of the database, some issues about the nature of the Metis data and the characteristic solar spatial scales involved in the observations need to be considered.

1. The coronal brightness imaged by Metis is a proxy for plasma density. It is in fact approximately defined, apart from geometrical factors, as the integral of the electron density along the line of sight (LOS; see, e.g., van de Hulst 1950). The measurements are integrated along the LOS so that smoothing of sharp gradients is in principle possible. However, it is understood that most of the white-light emission from the diffuse corona comes from the observed plane of the sky (POS; the generic plane orthogonal to the line of sight that corresponds to the plane onto which the image observed by a remote-sensing instrument is projected), especially for small radial distances (see, e.g., Howard & DeForest 2012, and following papers). As already highlighted in the literature by, e.g., Bemporad et al. (2008), Telloni et al. (2009a, 2013), and DeForest et al. (2018), integration along the LOS in the optically thin corona does not affect the spectral analysis of coronal fluctuations (and, in particular, the scaling of the observed power spectrum) as long as timescales of tens of minutes or longer are

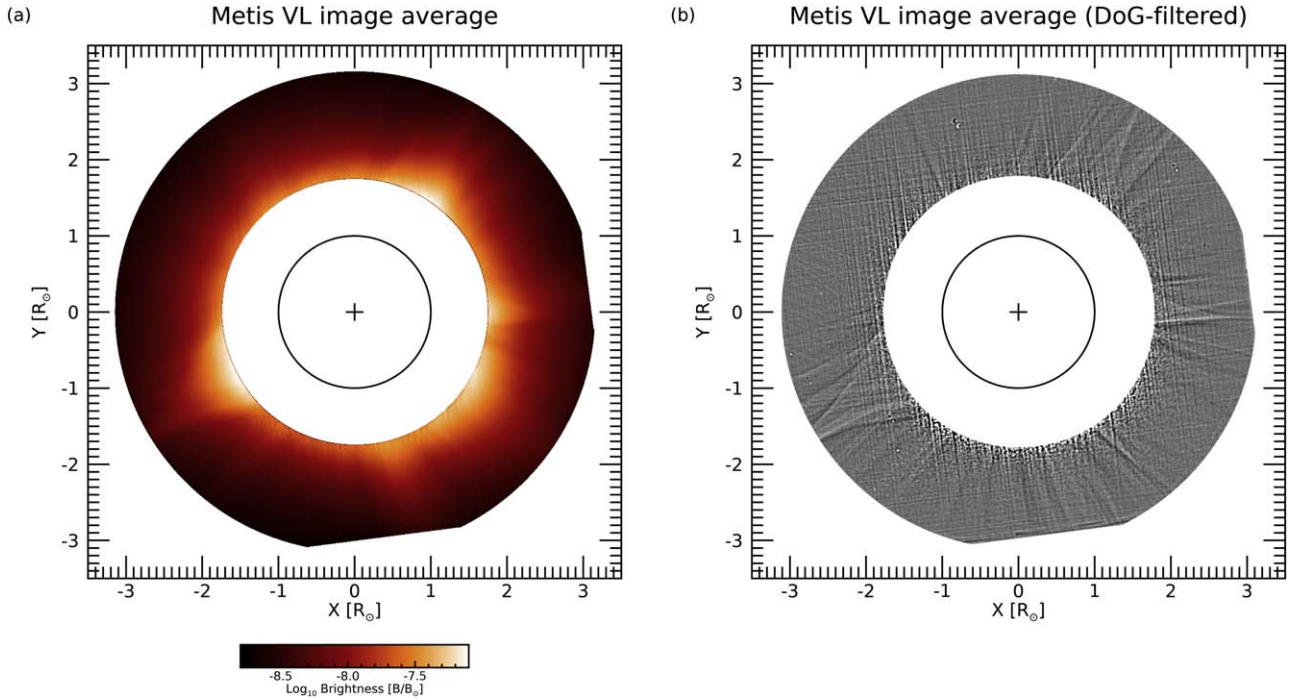


**Figure 1.** (a) Average of the 298 coronal brightness images acquired by Metis between 10:15 and 20:16 UT on 2022 October 12. (b) Same as (a), but with the DoG filter applied to sharpen the boundaries between different coronal magnetic structures.

considered. Therefore, fluctuations in the Metis time series can be considered as closely related to density fluctuations on the POS.

2. Metis provides a spatiotemporal sampling of the solar corona. Therefore, to determine the appropriate analysis, the nature of the measurements needs to be precisely established. In the maps collected by Metis, each pixel contains the local density at a given position in the corona as a function of time. The size of each pixel is approximately $6.2 \times 10^{-3}$ $R_\odot$ (~4300 km) on the POS. On the other hand, two successive measurements are separated by a cadence time of 2 minutes. Considering a typical coronal plasma outflow of $V \gtrsim 50$ km s$^{-1}$ (a sound assumption in the range of heights and latitudes considered here; see, e.g., Antonucci et al. 2005; Telloni et al. 2007; Antonucci et al. 2020a; Telloni et al. 2023b, except for any closed magnetic field regions), this corresponds to spatial scales larger than about 6000 km on the POS. Hence, two successive measurements in the same pixel do not pertain to the same plasma (a plasma parcel measured at one location traveled to at least nearly two pixels during one sample). Therefore, the time series at a given Metis image point provides radial flow measurements equivalent to those from an in situ probe standing at that position in the corona, with no overlap with the dynamical evolution of a given plasma element.
3. Classical turbulence theories are built on spatial fluctuations of the fields (e.g., Kolmogorov 1941; Frisch 1995). When using local fields measurements from in situ instruments onboard spacecraft, it is customary to invoke the Taylor hypothesis to convert time series to spatial profiles via the mean flow across the probe (Taylor 1938). At MHD scales, this requires that the bulk flow is fast enough to consider the fluctuations as frozen (or slowly evolving with respect to the relevant dynamical timescales of the system) during the measurement, at least in a statistical sense. Velocity measurements are not sufficiently resolved as to measure with precision the bulk speed ($V_0$) and the fluctuations ($\delta V$), so that a standard validation of the Taylor hypothesis ($\delta V/V_0 \ll 1$) cannot be performed. Therefore, it cannot be excluded that, at each pixel, the plasma flow dynamically evolves during the whole measurement interval. For this reason, the present analysis will be presented in the time domain, and interpretation in terms of turbulence models should be undertaken with caution. Hence, even if, according to Zank et al. (2022), the analysis performed here seems to be adequate for studying the properties of turbulence in the coronal regions imaged by Metis, the results can be interpreted in terms of turbulence theories only qualitatively.
4. The effects of solar rotation on Metis measurements are more important at low latitudes, while becoming negligible toward the poles. Specifically, during the time of one sample, the solar source of the plasma seen by Metis will be rotating by approximately $0\overset{\circ}{.}0093$ at the equator (the Sun's rotation is seen as effectively slowed down by Metis because of the high longitudinal velocity of Solar Orbiter at perihelion). This corresponds to spatial structures of approximately 113 km at the equator on the photosphere. A 30 minute Metis time series will thus correspond to a longitudinal scan of $0\overset{\circ}{.}14$ or 1700 km on the photosphere at the equator, and the full observation of 10 hr to $2\overset{\circ}{.}8$ or 34,000 km (=0.049 $R_\odot$). Typical photospheric structures include granulation, mesogranulation,[42] and supergranulation. These have typical scales

[42] Although mesogranulation is not universally recognized as an effective convective scale on the Sun, but rather the result of a "cooperative interaction" between small scales and photospheric fluxes (see, e.g., Rincon & Rieutord 2018), its reference in the text is useful only for the purpose of identifying the (meso)scales involved in Metis observations.

of 1000, 5000–10,000, and 30,000 km, and average lifetimes of 0.2, 3, and 20 hr, respectively (e.g., Rast 2003, and references therein). Hence, the full Metis database can scan up to approximately one supergranule, while each snapshot scans $\sim 1/10$ of a granule. A 1 hr interval (or timescale) would finally correspond to 3–4 granules, or slightly less than one mesogranule. It follows that in the range of timescales between 1 and 10 hr, Metis is in principle sensitive to density fluctuations induced by mesogranulation dynamics.

5. As evidenced by an analysis on uncalibrated Metis images, the physical signal-related fluctuations were found to be significantly larger, at all the frequencies involved, than those associated with the instrument's electronic noise (appearing as a gridlike pattern in Figure 1(b)), thus effectively ruling out the possibility that read-out noise could affect the spectra of brightness fluctuations (and, in turn, their scaling). More specifically, the spectral responses of the coronal signal and the signal within the occulted region of the solar disk (clearly due solely to the instrument electronics) were compared. It was found that the Metis instrumental noise becomes significant only on timescales smaller than 10 minutes. Since the scales involved in the analysis range from 1 to 10 hr, and are thus 1 order of magnitude larger, it follows that the results are not affected by instrumental noise. It is further worth noting that the Poissonian-type uncertainties associated with 2 minute measurements of total brightness from Metis are less than 10%. Therefore, the relative error associated with hourly averages, and thus with the timescales considered in this work, is reduced to below 2%.
6. A final note concerns the possibility of transient events in the database. For example, at least one (faint) coronal mass ejection (CME) occurred during the analyzed period. However, sporadic events are not expected to affect the scaling of the power spectrum of interest in this work. This has been proven by showing that the results of the analysis presented below do not change when excluding the portion of the POS interested by the CME (not shown). On the other hand, periodic events such as those investigated by Ventura et al. (2023) should appear as frequency peaks superposed on the background fluctuation spectrum, though not altering its slope.

It turns out that, albeit indirectly and with some layers of approximation, the spectral analysis of Metis coronal brightness measurements is appropriate to investigate the turbulent state of the solar corona driven by mesogranular-scale photospheric dynamics.

Several techniques can be used to extract information about the statistical properties of the density fluctuations. Based on the above discussion, each pixel provides a 298-point time series that can be analyzed using standard diagnostics to provide the temporal characteristics of the measurements. The scales of interest for this work, sitting above 1 hr and up to the 10 hr observation duration, do not include the time variability of the plasma in each pixel, but rather spatial fluctuations related to density structures transported by the coronal flow. The first analysis performed is the frequency spectrum $E(f)$, obtained through a standard Fourier transform, of the time series for each pixel. If a power-law scaling is present, as is often the case in turbulent or noisy data, the spectral index $\alpha$ can be estimated as $E(f) \propto f^{\alpha}$. An equivalent measure of the same scaling exponent can be obtained through the second-order structure function, $S_2(\Delta t) = \langle \Delta\rho^2 \rangle \propto \Delta t^{\zeta_2}$, where $\Delta\rho = \rho(t + \Delta t) - \rho(t)$ are the scale-dependent density increments across the timescale $\Delta t$. A relation between the two exponents exists, $\alpha = -(\zeta_2 + 1)$. The spectral index and the second-order structure function exponents are both related to the global self-similarity properties of the field, which in the Kolmogorov phenomenological theory of turbulence determine the scaling of the statistical properties of the fluctuations.

Maps of the values of the structure functions at timescales of 1, 2, 4, and 8 hr are displayed in Figures 2(a)–(d), respectively. A map of the exponent $\alpha = -(\zeta_2 + 1)$ as measured using $S_2$ and relative to the 1 hr $\leqslant \Delta t \leqslant$ 10 hr spectral range is instead presented in Figure 3(a).

The evident inhomogeneity and strong local variability of such maps reveal the complex nature of the coronal density fluctuations. Specifically, Figure 2 visibly shows the appearance of filamentary, nearly radial structures, which highlight the typical shape of the stronger coronal magnetic field lines. In particular, the density fluctuations are enhanced along the field lines, with their amplitude increasing with $\Delta t$, thus identifying a coupling between fluctuating density structures and coronal magnetic field patterns. This result is well known in the literature and discussed extensively in, e.g., Telloni et al. (2013) and DeForest et al. (2018). The spectral exponents (Figure 3(a)) are steeper (and relatively constant) along such structures, where typically $\alpha \lesssim -2$ (this is particularly prominent at the edge marking the boundary between the streamer-shaped magnetic structure and the open magnetic field region at the southeastern solar limb). This suggests that the stronger coronal magnetic field might be inhibiting the turbulent nonlinear interactions, maintaining the large fluctuations closer to random. However, as noted in point 3 in Section 2, the possible role of entangled spatial structure and dynamical evolution cannot be excluded.

It is also worth noting that the spatial distribution of $\alpha$ is unrelated to the large-scale configuration of the corona (Figure 1(a)). Indeed, neither streamers nor open-field regions associated with coronal holes are evident in the spectral index map in Figure 3(a). Specifically, $\alpha$ values close to $-1$ (suggestive of noise) are not systematically observed in low-density regions, where the coronal signal is weaker. On the other hand, $\alpha$ values close to or lower than $-2$ are not only observed in low-latitude high-density regions, where they could be interpreted as due to discontinuities crossing the single pixel during solar rotation. Instead, they are also found, for example, in the low-density northern polar coronal hole, where the effect of solar rotation is negligible. This indicates that (i) the rotation does not affect the results and (ii) the less dense regions are not affected by the Metis instrumental noise (as discussed above, this involves timescales 1 order of magnitude smaller than those under study).

The full corona image time series can be considered as an ensemble of a turbulent system. The high latitudinal variability of the scaling exponents, which can be interpreted, in principle, as due to the local inhomogeneity of the coronal flow source regions, is an indication that the corona is, overall, a multifractal structure (i.e., the corona is characterized by physical processes governed by multiple scaling laws). At the closest distance from the Sun, each pixel covers a 0°.2 latitudinal span, which corresponds to $\sim$2500 km on the solar

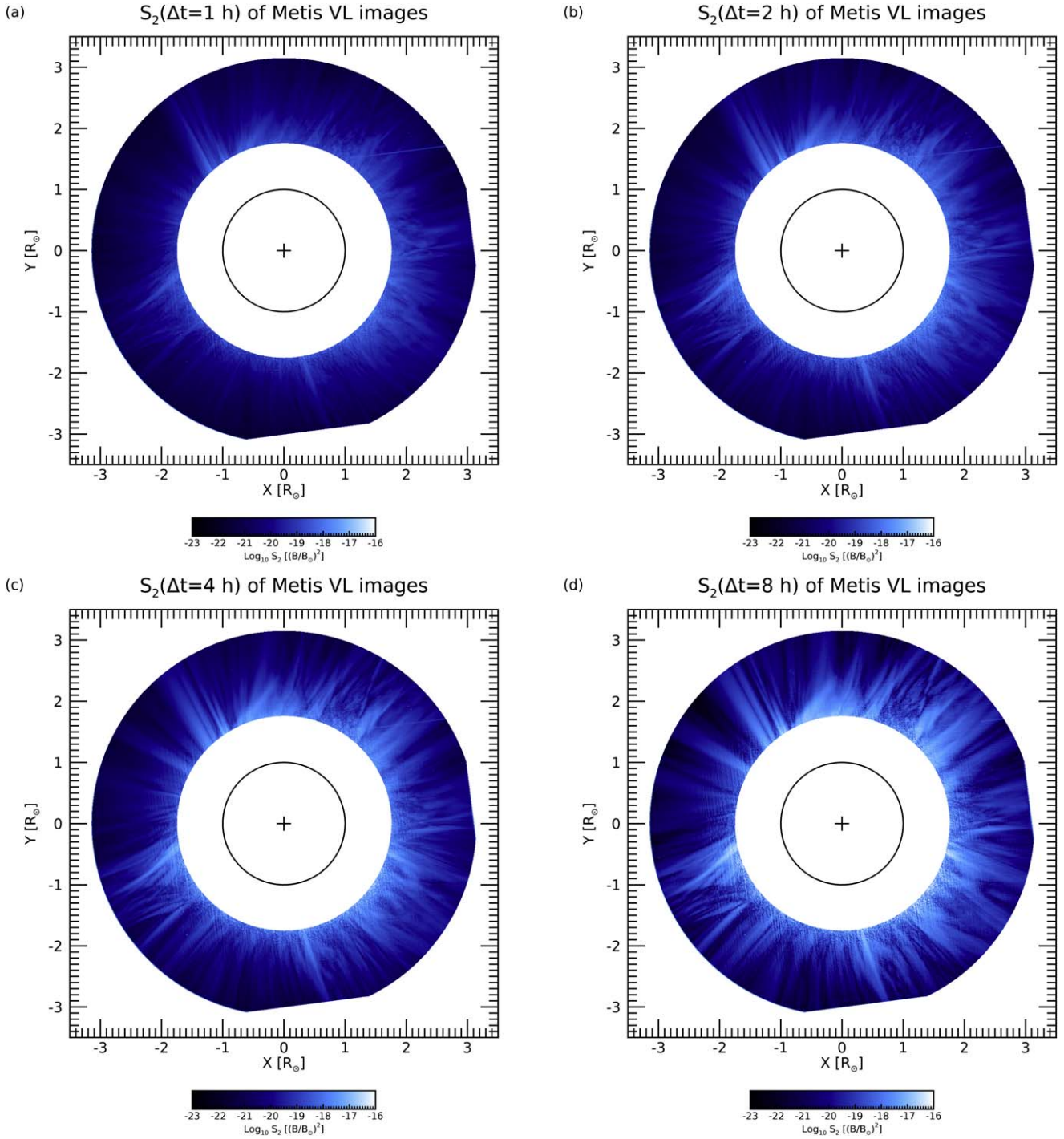


**Figure 2.** Second-order structure functions $S_2$ at the lag $\Delta t$ of 1 hr (a), 2 hr (b), 4 hr (c), and 8 hr (d), computed from the series of Metis VL images in the whole FOV of the detector.

photosphere, namely the size of a couple of granules. At a fixed distance $r$ from the Sun, a circular profile extracted from the exponent map will thus provide the latitudinal variability of the density fluctuations' statistical properties. Figure 3(b) shows the spectral index values estimated along a circular profile for four different radial distances $r$ from the Sun (1.8, 2.2, 2.6, and 3.0 $R_\odot$, marked by different-colored dashed circles in Figure 3(a)) and collected in histograms, with mean and standard deviation reported in the legend. The $\alpha$ distributions are roughly Gaussian (though slightly negatively skewed) at all distances from the Sun. However, the normalized rms deviation (i.e., the ratio of the standard deviation to the mean) increases moving away from the Sun (from 0.11 at 1.8 $R_\odot$ to 0.19 at 3.0 $R_\odot$), that is, the distributions are broader far from the Sun, indicating a more inhomogeneous plasma there. It appears then evident that the mean spectral index decreases from 2.32 to $1.64 \simeq 5/3$ over the altitude range covered by the Metis observations. This seems to indicate a transition from relatively smooth to more disordered fluctuations, with the exponents at larger distances reaching values compatible with a Kolmogorov picture of turbulence. The radial evolution of the density fluctuations (whose average variance at the largest scale

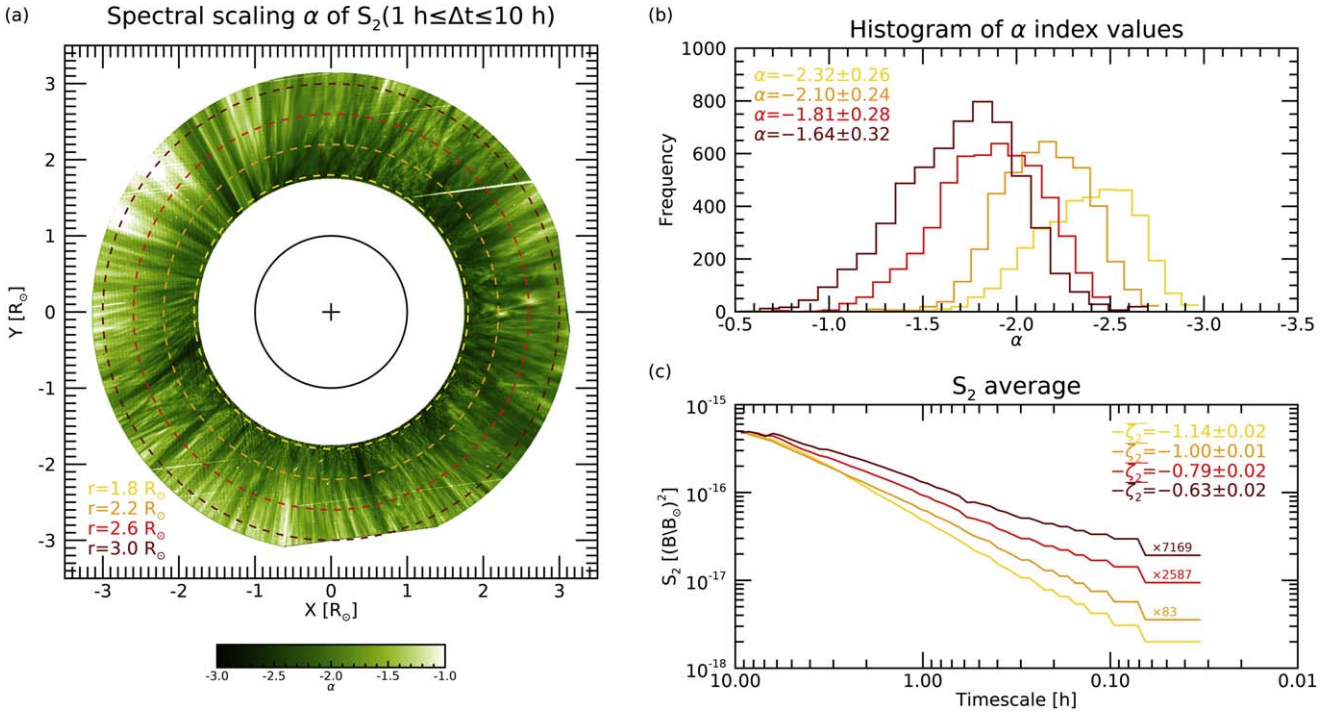


**Figure 3.** (a) Map of the spectral index $\alpha = -(\zeta_2 + 1)$ derived from the second-order structure functions $S_2$ in the scale range from $\Delta t = 1$ to $\Delta t = 10$ hr. (b) Distributions of the ensembles of $\alpha$ values extracted from the polar profiles at 1.8, 2.2, 2.6, and 3.0 $R_\odot$, indicated with color-coded, dashed circles in (a); the mean and standard deviation of each distribution are also reported. (c) Averages of the second-order structure functions $S_2$ obtained along the same circular profiles and displayed in the same color scheme (the curves are downscaled, according to the indicated values, to retain the same value at the largest timescale of 10 hr for easy comparison of the corresponding scaling laws); the exponents $-\overline{\zeta_2}$ computed from power-law fitting in the 1 hr $\leqslant \Delta t \leqslant$ 10 hr range (along with the corresponding uncertainties) are also shown.

decreases from $8.7 \times 10^{-19}$ $(B/B_\odot)^2$ at 1.8 $R_\odot$ to $4.3 \times 10^{-21}$ $(B/B_\odot)^2$ at 3.0 $R_\odot$) seems, therefore, to show a transition to fully developed turbulence, which, on average, appears to be set at a distance of 3 $R_\odot$ from the Sun. This is the height at which, according to the potential field source surface models (Altschuler & Newkirk 1969; Schatten et al. 1969), the plasma dynamics would begin to dominate over the magnetic field. This evidence is corroborated by the structure functions averaged over the same polar profiles (shown in Figure 3(c) and downscaled to the value corresponding to $\Delta t = 10$ hr for easier comparison) and by deriving the scaling exponents over the scale range of interest. Note that the two procedures lead to slightly different values for the spectral indices (averaging the scaling exponents derived from different spectra is not the same as deriving the scaling exponent from an average spectrum). Nonetheless, it can be seen that the second-order structure functions become less steep at larger distances from the Sun, approaching the Kolmogorov reference at 3 $R_\odot$, thus suggesting the onset of fully developed turbulence in the solar corona at around such height. The flattening of spectra for timescales of less than a dozen minutes provides evidence that the Metis instrumental noise affects only this range of small scales. Also interesting (though beyond the scope of the present work) is noting the slight spectral break at about 0.2–0.3 hr. Although this might be due to the Metis background noise flattening the spectrum or to the failure of the Taylor hypothesis, evidence of this occurring at the timescale characteristic of granulation suggests further analysis.

## 3. Conclusions

The results illustrated in this Letter provide important elements to understand the origin, evolution, and transport of solar wind turbulence, and ultimately the coronal heating, in the framework of state-of-the-art MHD turbulence models. The Kolmogorov phenomenological predictions have been previously observed in the density field of both the interplanetary (using in situ measurements; e.g., Telloni et al. 2009b) and interstellar (using remote-sensing radio scintillation observations; Armstrong et al. 1981) medium. Turbulent features above the solar corona, in the very inner heliosphere, have also been reported in DeForest et al. (2016). The present analysis complements these observations with the case of the near-Sun plasma and suggests the coronal origin of solar wind turbulence.

The lack of sufficiently resolved velocity fluctuations prevents a full evaluation of the conditions for the validity of the Taylor hypothesis. Therefore, the analysis presented here should be considered as an assessment of the sole time-domain turbulence properties. Nevertheless, when ensemble-averaging over latitude, a power-law scaling is observed for the time-based second-order structure functions, at timescales between 1 and 10 hr. The equivalent spectral exponents increase from $-2.32$ to $-1.64$ when moving radially from 1.8 to 3 $R_\odot$, regardless of the portion of the observed solar corona (low- or high-density regions). As discussed above, this is not due to either methodological or instrumental noise issues. The $-5/3$ exponent found at the outermost height is compatible with typical Kolmogorov phenomenology in space plasmas and suggests that the plasma density might be experiencing a transition to fully developed turbulence in the observed range. A similar transition is observed, for example, in the terrestrial magnetosheath downstream of the bow shock (Yordanova et al. 2008). Spacecraft measurements show that the shock crossing initially destroys the solar-wind preexisting turbulence,

producing fluctuations with steep ($\alpha \simeq -2.5$) spectra and self-similar statistics, which then evolve to the standard Kolmogorov value and develop intermittency (see Sahraoui et al. 2020, and references therein). A $5/3$ spectral scaling in the density fluctuations was also found by analyzing the Parker Solar Probe plasma data during the spacecraft's incursions into the solar corona. Therefore, the present results are in agreement with in situ measurements. Note however that, unlike in the present case, in the mentioned systems the Taylor hypothesis is usually verified.

Assuming that the temporal analysis provides a reasonable representation of the spatial properties of turbulence (see Zank et al. 2022), it is possible to compare the observations presented here with models of MHD turbulence. The predicted density spectra $E_\rho(k_\perp, k_\parallel)$ (with $k_\perp$ and $k_\parallel$ being the wavenumber perpendicular and parallel to the mean magnetic field, respectively) have been discussed quite extensively in Zank et al. (2017, 2022). The density fluctuation spectral density is shown to depend on the value of the 2D residual energy.[43] If it is either balanced kinetic and magnetic 2D energy or all kinetic energy, then $E_\rho(k_\perp) \propto k_\perp^{-5/3}$, assuming isotropy and provided that the underlying 2D turbulence is Kolmogorov-like (see, in particular, Equation (55) in Zank et al. 2017, and the related discussion). A direct link with the Elsässer 2D $k_\perp^{-5/3}$ spectrum can thus be recovered in this case. It follows that, as mentioned above, the density fluctuations can be regarded as transported coronal structures, which furthermore do not affect the turbulent scaling laws for Elsässer fields. The Kolmogorov spectrum for density fluctuations at 3 $R_\odot$ thus reflects the underlying quasi-2D incompressible turbulence and predicts that this is likely balanced at such a distance from the Sun. This suggests either that the density, magnetic, and velocity fluctuations evolve from 1 to 3 $R_\odot$ into a fully turbulent state or, alternatively, that the residual energy changes with distance as well. As a corollary, this method should be more sensitive to Alfvénic (slab) than to 2D fluctuations. However, spatial information (comparison across pixels) could clearly identify 2D density fluctuations.

A mode-decomposition analysis (based on the diagnostics advanced by Zank et al. 2023, and which is the subject of a work currently ongoing) of the first time interval when Parker Solar Probe was immersed in the solar corona, suggests that the entropy (density) fluctuations are the dominant component and follow a $k^{-5/3}$ spectrum, in agreement with the present study.

Further investigations are needed for disentangling the role of photospheric spatial dynamics from the temporal variability of the coronal flow source regions, as well as the effects of solar rotation in a nonstationary and highly inhomogeneous environment such as the Sun's atmosphere, in order to understand coronal turbulence in greater detail. Analyses such as the spatial 2D spectrum for a given time instant $t$, $k - \omega$ spectra, kurtosis (largely used to study intermittency, a characteristic feature of turbulence; see Frisch 1995), and proper orthogonal decomposition (Vecchio et al. 2005) are all useful diagnostic tools in coming to a better description of coronal density fluctuations in the context of current turbulence theories. Some of these studies are in progress and will be addressed in forthcoming papers.

[43] Residual energy quantifies the imbalance between magnetic and kinetic energy.


## Acknowledgments

Solar Orbiter is a space mission of international collaboration between ESA and NASA, operated by ESA. D.T. was partially supported by the Italian Space Agency (ASI) under contract 2018-30-HH.0. L.S.-V. was supported by the Swedish Research Council Research Grant 2022-03352. G.P.Z., L.A., and L.-L.Z. acknowledge the partial support of a NASA Parker Solar Probe contract SV4-84017, an NSF EPSCoR RII-Track-1 Cooperative Agreement OIA-2148653, and a NASA IMAP grant through SUB000313/80GSFC19C0027. S.G. acknowledges the financial support of the Programma Operativo Nazionale (PON) "Ricerca e Innovazione" 2014-2020. F.C. is a PhD student with a fellowship of the National Institute for Astrophysics. P.H. acknowledges support from the grant 22-34841S of the Czech Science Foundation and he was also supported by the program "Excellence Initiative—Research University" for the years 2020–2026 at the University of Wrocław, project No. BPIDUB.4610.96.2021.KG. L.S. was supported by a grant from the NASA Heliophysics Technology and Instrument Development for Science Program, NNH15ZDA001N-HTIDS, and also by the basic Research Funds of the Office of Naval Research. The Metis program is supported by ASI under contracts to the National Institute for Astrophysics and industrial partners. Metis was built with hardware contributions from Germany (Bundesministerium für Wirtschaft und Energie through the Deutsches Zentrum für Luft- und Raumfahrt e.V.), the Czech Republic (PRODEX), and ESA. The Metis data analyzed in this Letter are available from the PI on request.



## ORCID iDs

Daniele Telloni https://orcid.org/0000-0002-6710-8142
Luca Sorriso-Valvo https://orcid.org/0000-0002-5981-7758
Gary P. Zank https://orcid.org/0000-0002-4642-6192
Marco Velli https://orcid.org/0000-0002-2381-3106
Vincenzo Andretta https://orcid.org/0000-0003-1962-9741
Denise Perrone https://orcid.org/0000-0003-1059-4853
Raffaele Marino https://orcid.org/0000-0002-6433-7767
Francesco Carbone https://orcid.org/0000-0002-3559-5273
Antonio Vecchio https://orcid.org/0000-0002-2002-1701
Laxman Adhikari https://orcid.org/0000-0003-1549-5256
Lingling Zhao https://orcid.org/0000-0002-4299-0490
Sabrina Guastavino https://orcid.org/0000-0001-7047-1148
Fabiana Camattari https://orcid.org/0009-0002-5200-644X
Chen Shi https://orcid.org/0000-0002-2582-7085
Nikos Sioulas https://orcid.org/0000-0002-1128-9685
Zesen Huang https://orcid.org/0000-0001-9570-5975
Marco Romoli https://orcid.org/0000-0001-9921-1198
Ester Antonucci https://orcid.org/0000-0003-4155-6542
Vania Da Deppo https://orcid.org/0000-0001-6273-8738
Silvano Fineschi https://orcid.org/0000-0002-2789-816X
Catia Grimani https://orcid.org/0000-0002-5467-6386
Petr Heinzel https://orcid.org/0000-0002-5778-2600
John D. Moses https://orcid.org/0000-0001-9670-2063
Giampiero Naletto https://orcid.org/0000-0003-2007-3138
Gianalfredo Nicolini https://orcid.org/0000-0002-9459-3841
Daniele Spadaro https://orcid.org/0000-0003-3517-8688
Marco Stangalini https://orcid.org/0000-0002-5365-7546
Luca Teriaca https://orcid.org/0000-0001-7298-2320
Michela Uslenghi https://orcid.org/0000-0002-7585-8605
Lucia Abbo https://orcid.org/0000-0001-8235-2242
Frédéric Auchère https://orcid.org/0000-0003-0972-7022

Regina Aznar Cuadrado https://orcid.org/0000-0003-1294-1257
Arkadiusz Berlicki https://orcid.org/0000-0002-6505-4478
Roberto Bruno https://orcid.org/0000-0002-2152-0115
Aleksandr Burtovoi https://orcid.org/0000-0002-8734-808X
Gerardo Capobianco https://orcid.org/0000-0003-0520-2528
Chiara Casini https://orcid.org/0000-0001-8783-0047
Marta Casti https://orcid.org/0000-0002-9716-3820
Paolo Chioetto https://orcid.org/0000-0002-3379-2142
Alain J. Corso https://orcid.org/0000-0003-0378-9249
Raffaella D'Amicis https://orcid.org/0000-0003-2647-117X
Yara De Leo https://orcid.org/0000-0003-2426-2112
Michele Fabi https://orcid.org/0000-0002-2464-1369
Federica Frassati https://orcid.org/0000-0001-9014-614X
Fabio Frassetto https://orcid.org/0000-0001-5528-1995
Silvio Giordano https://orcid.org/0000-0002-3468-8566
Salvo L. Guglielmino https://orcid.org/0000-0002-1837-2262
Giovanna Jerse https://orcid.org/0000-0002-0764-7929
Federico Landini https://orcid.org/0000-0001-8244-9749
Alessandro Liberatore https://orcid.org/0000-0002-0016-7594
Enrico Magli https://orcid.org/0000-0002-0901-0251
Giuseppe Massone https://orcid.org/0000-0002-2656-1557
Giuseppe Nisticò https://orcid.org/0000-0003-2566-2820
Maurizio Pancrazzi https://orcid.org/0000-0002-3789-2482
Maria G. Pelizzo https://orcid.org/0000-0002-1383-6750
Hardi Peter https://orcid.org/0000-0001-9921-0937
Christina Plainaki https://orcid.org/0000-0003-1483-5052
Luca Poletto https://orcid.org/0000-0002-0914-0531
Fabio Reale https://orcid.org/0000-0002-1820-4824
Paolo Romano https://orcid.org/0000-0001-7066-6674
Giuliana Russano https://orcid.org/0000-0002-2433-8706
Clementina Sasso https://orcid.org/0000-0002-5163-5837
Udo Schühle https://orcid.org/0000-0001-6060-9078
Sami K. Solanki https://orcid.org/0000-0002-3418-8449
Leonard Strachan https://orcid.org/0000-0002-5425-7122
Thomas Straus https://orcid.org/0000-0002-6280-806X
Roberto Susino https://orcid.org/0000-0002-1017-7163
Rita Ventura https://orcid.org/0000-0002-5152-0482
Cosimo A. Volpicelli https://orcid.org/0000-0002-4997-1460
Joachim Woch https://orcid.org/0000-0001-5833-3738
Luca Zangrilli https://orcid.org/0000-0002-4184-2031
Gaetano Zimbardo https://orcid.org/0000-0002-9207-2647
Paola Zuppella https://orcid.org/0000-0003-0290-3193

## References

Altschuler, M. D., & Newkirk, G. 1969, SoPh, 9, 131
Antonucci, E., Abbo, L., & Dodero, M. A. 2005, A&A, 435, 699
Antonucci, E., Harra, L., Susino, R., & Telloni, D. 2020a, SSRv, 216, 117
Antonucci, E., Romoli, M., Andretta, V., et al. 2020b, A&A, 642, A10
Armstrong, J. W., Cordes, J. M., & Rickett, B. J. 1981, Natur, 291, 561
Bemporad, A., Matthaeus, W. H., & Poletto, G. 2008, ApJL, 677, L137
Bohr, T., Jensen, M. H., Paladin, G., & Vulpiani, A. 1998, Dynamical Systems Approach to Turbulence (Cambridge: Cambridge Univ. Press)
Bruno, R., & Carbone, V. 2013, LRSP, 10, 2
Carbone, F., Alberti, T., Faranda, D., et al. 2022a, PhRvE, 106, 064211
Carbone, F., Gencarelli, C. N., & Hedgecock, I. M. 2016, PhRvE, 94, 063101
Carbone, F., Telloni, D., Zank, G., & Sorriso-Valvo, L. 2021, PhRvE, 104, 025201
Carbone, F., Telloni, D., Zank, G., & Sorriso-Valvo, L. 2022b, EL, 138, 53001
Chhiber, R., Usmanov, A. V., Matthaeus, W. H., & Goldstein, M. L. 2019, ApJS, 241, 11
Coleman, P. J. J. 1968, ApJ, 153, 371
De Leo, Y., Burtovoi, A., Teriaca, L., et al. 2023, A&A, 676, A45
DeForest, C. E., Howard, R. A., Velli, M., Viall, N., & Vourlidas, A. 2018, ApJ, 862, 18
DeForest, C. E., Matthaeus, W. H., Viall, N. M., & Cranmer, S. R. 2016, ApJ, 828, 66
Domingo, V., Fleck, B., & Poland, A. I. 1995, SoPh, 162, 1
Federrath, C., & Klessen, R. S. 2012, ApJ, 761, 156
Feynman, R. P., Leighton, R. B., & Matthew, S. 1963, The Feynman Lectures on Physics—Volume 1 (Reading, MA: Addison–Wesley)
Fineschi, S., Naletto, G., Romoli, M., et al. 2020, ExA, 49, 239
Fox, N. J., Velli, M. C., Bale, S. D., et al. 2016, SSRv, 204, 7
Frisch, U. 1995, Turbulence. The Legacy of A.N. Kolmogorov (Cambridge: Cambridge Univ. Press)
Gallavotti, G., & Cohen, E. G. D. 1995, PhRvL, 74, 2694
Howard, T. A., & DeForest, C. E. 2012, ApJ, 752, 130
Huang, Y., & Wang, L. 2019, PhyS, 94, 014009
Hundhausen, A. J. 1972, Coronal Expansion and Solar Wind (Berlin: Springer)
Kasper, J. C., Klein, K. G., Lichko, E., et al. 2021, PhRvL, 127, 255101
Kohl, J. L., Esser, R., Gardner, L. D., et al. 1995, SoPh, 162, 313
Kolmogorov, A. 1941, DoSSR, 30, 301
Kritsuk, A. G., Norman, M. L., & Wagner, R. 2011, ApJL, 727, L20
Liberatore, A., Fineschi, S., Casti, M., et al. 2023, A&A, 672, A14
Lotova, N. A., Blums, D. F., & Vladimirskii, K. V. 1985, A&A, 150, 266
Marino, R., Feraco, F., Primavera, L., et al. 2022, PhRvF, 7, 033801
Marino, R., & Sorriso-Valvo, L. 2023, PhR, 1006, 1
Matthaeus, W. H., Zank, G. P., Oughton, S., Mullan, D. J., & Dmitruk, P. 1999, ApJL, 523, L93
Morgan, H., & Druckmüller, M. 2014, SoPh, 289, 2945
Morgan, H., Habbal, S. R., & Li, X. 2004, ApJ, 605, 521
Müller, D., St., Cyr, O. C., Zouganelis, I., et al. 2020, A&A, 642, A1
Ofman, L., Romoli, M., Poletto, G., Noci, G., & Kohl, J. L. 2000, ApJ, 529, 592
Rast, M. P. 2003, ApJ, 597, 1200
Réville, V., & Brun, A. S. 2017, ApJ, 850, 45
Rincon, F., & Rieutord, M. 2018, LRSP, 15, 6
Sahraoui, F., Hadid, L., & Huang, S. 2020, RvMPP, 4, 4
Schatten, K. H., Wilcox, J. M., & Ness, N. F. 1969, SoPh, 6, 442
Schekochihin, A. A., & Cowley, S. C. 2006, PhPl, 13, 056501
Taylor, G. I. 1938, RSPSA, 164, 476
Telloni, D., Antonucci, E., Bruno, R., & D'Amicis, R. 2009a, ApJ, 693, 1022
Telloni, D., Antonucci, E., & Dodero, M. A. 2007, A&A, 476, 1341
Telloni, D., Antonucci, E., Dolei, S., et al. 2014, A&A, 565, A22
Telloni, D., Bruno, R., Carbone, V., Antonucci, E., & D'Amicis, R. 2009b, ApJ, 706, 238
Telloni, D., Ventura, R., Romano, P., Spadaro, D., & Antonucci, E. 2013, ApJ, 767, 138
Telloni, D., Sorriso-Valvo, L., Woodham, L. D., et al. 2021, ApJL, 912, L21
Telloni, D., Romoli, M., Velli, M., et al. 2023a, ApJL, 955, L4
Telloni, D., Antonucci, E., Adhikari, L., et al. 2023b, A&A, 670, L18
Title, A. M., & Schrijver, C. J. 1998, ASP Conf. Ser. 154, Cool Stars, Stellar Systems, and the Sun, ed. R. A. Donahue & J. A. Bookbinder (San Francisco, CA: ASP), 345
Tu, C. Y., & Marsch, E. 1995, SSRv, 73, 1
van de Hulst, H. C. 1950, BAN, 11, 135
Vecchio, A., Carbone, V., Lepreti, F., et al. 2005, PhRvL, 95, 061102
Velli, M. 1993, A&A, 270, 304
Ventura, R., Antonucci, E., Downs, C., et al. 2023, A&A, 675, A170
Verdini, A., Velli, M., & Buchlin, E. 2009, ApJL, 700, L39
Verscharen, D., Klein, K. G., & Maruca, B. A. 2019, LRSP, 16, 5
Viavattene, G., Consolini, G., Giovannelli, L., et al. 2020, Entrp, 22, 716
Viavattene, G., Murabito, M., Guglielmino, S. L., et al. 2021, Entrp, 23, 413
Yordanova, E., Vaivads, A., André, M., Buchert, S. C., & Vörös, Z. 2008, PhRvL, 100, 205003
Zank, G. P., Adhikari, L., Hunana, P., et al. 2017, ApJ, 835, 147
Zank, G. P., Adhikari, L., Hunana, P., et al. 2018, ApJ, 854, 32
Zank, G. P., Nakanotani, M., Zhao, L. L., Adhikari, L., & Telloni, D. 2020, ApJ, 900, 115
Zank, G. P., Zhao, L. L., Adhikari, L., et al. 2023, ApJS, 268, 18
Zank, G. P., Zhao, L. L., Adhikari, L., et al. 2021, PhPl, 28, 080501
Zank, G. P., Zhao, L. L., Adhikari, L., et al. 2022, ApJL, 926, L16
Zhao, L. L., Zank, G. P., Telloni, D., et al. 2022, ApJL, 928, L15